Active and Passive Elec. Comp., 1995, Vol. 18, pp. 39–51
Reprints available directly from the publisher
Photocopying permitted by license only

© 1995 OPA (Overseas Publishers Association)
Amsterdam B.V. Published under license by
Gordon and Breach Science Publishers SA
Printed in Malaysia

A NEW METHOD FOR THE PREPARATION OF FINE-GRAINED SnO_2 AND WO_3 POWDERS: INFLUENCE OF THE CRYSTALLITE SIZE ON THE ELECTROCHEMICAL INSERTION OF Li^+ IN SnO_2 AND WO_3 ELECTRODES

S.D. HAN, G. CAMPET*, S.Y. HUANG, M.C.R. SHASTRY AND J. PORTIER

Laboratoire de Chimie du Solide du CNRS, Université Bordeaux I, 351 Cours de la Libération, 33405 Talence cedex, FRANCE.

J.C. LASSÈGUES

Laboratoire de Spectroscopie Moléculaire et Cristalline, Université Bordeaux I, 351 Cours de la Libération, 33405 Talence cedex, FRANCE.

H.S. DWEIK

AL-Quds University, College of Science & Technology, Jerusalem; West Bank

(Received November 20, 1994; in final form November 30, 1994)

We propose an unconventional method to obtain fine-grained SnO_2 and WO_3 powders. It uses as precursors, polymer complexes between polyethylene oxide (POE) and $SnCl_4$ or WCl_6 respectively. By pyrolysis of these complexes in the 350-550°C temperature range, metal-oxide powders possessing small crystallite sizes are obtained. They are free from water and hydroxyl group contaminations, which is an added advantage where the application of these materials to Li-batteries is concerned. We have, indeed, demonstrated that these powders show good ability to insert reversibly lithium ions in the $Li/Li^+/SnO_2$ (WO_3) cells.

INTRODUCTION

SnO_2 is an *n*-type semiconductor with a tetragonal rutile structure[1] and a large indirect band energy gap (2.7 eV)[2]. It has attracted considerable attention to the variety of applications related to its unique electrical, optical and catalytic properties. Among its applications, to mention only a few, are in transparent heaters for windshield defrosting, in anti-reflection coating for solar cells, as a transparent electrode for electrochromic devices, as a sensing material for combustible gas sensors, and as an electrocatalyst for organic oxidation[3-8]. In the last two applications mentioned above, fine powders of SnO_2 are used. These powders have generally been obtained through two different methods: one involves the oxidation of elemental tin with acids (HNO_3, H_2SO_4 etc.) and the other utilizes the well-known sol-gel route. The sol-gel method involves the dispersion of stannic hydrate in aqueous ammonia to give a sol. The sol is later 'solidified' through stages of stiffening and polymerization to give a gel (gelation). The gel so obtained is

*Author for correspondence

*Present address: Institut de Chemie de la Matièra Condensée de Bordeaux, CNRS, Université Bordeaux I, Chateau Brivazac, Ave du Dr. A. Schweitzer, 33600 Pessac, France.

thoroughly washed with distilled water, filtered, dried and finally heated to high temperatures to obtain the required material[9]. The sol-gel route has been found to give finer crystallites compared to the former method. However, samples free from water and hydroxyl groups are hardly achievable when low calcination temperatures are used.

WO_3 is an *n*-type semiconductor that displays three crystal polytypes: monoclinic, hexagonal and orthorhombic[10]. WO_3 powders can be obtained using the same preparation procedure used for SnO_2. They have also been prepared using other techniques. Cheng et al.[11-12] obtained WO_3 powders from the thermal decomposition of ammonium paratungstate while Zhong et al.[13] used a similar process with H_2WO_4. These authors were primarily concerned with making cathode electrodes for secondary lithium batteries where high surface area is an important parameter. The specific surface areas of the WO_3 powders obtained from the thermal decomposition of H_2WO_4 were between 12.2 and 4.3 m^2/g[13], and so were of limited use for this purpose. Low specific surface areas are obtained not only for the WO_3 powders but also for the SnO_2 powders obtained using the preparation procedures quoted above. There is, therefore, a need to develop a method to produce WO_3 and SnO_2 powders with higher surface areas for use as cathode materials in lithium electrochemical cells. For this purpose the powders will also have to be free of water and hydroxyl groups.

We propose here an unconventional and easy-to-carry-out method for the preparation of fine particles of SnO_2 and WO_3 powders. It uses as precursors complexes of the respective halides $SnCl_4$ and WCl_6 with polyethylene oxide (PEO)[14]. The method has been shown to give not only very fine particles, obtained after eliminating the polymer by heating, but also particles free from water and OH group impurities.

The conventional and unconventional sol-gel methods will be compared here; they will be referred to as method 1 (for the conventional one) and method 2.

We also investigated the ability to insert reversibly lithium ions into the fine-grained SnO_2 and WO_3 powders in $Li/Li^+/SnO_2$ (WO_3) electrochemical cells. Related to that, we have reported elsewhere that electrodes based on fine-grained transitions metal oxides ($Li_xFe_2O_3$, $Li_{2-X}NiO_2$ etc.) in the form of thin films exhibit highly efficient electrochemical (de)insertion of Li^+ ions into lithium conducting electrolytes[15-17]. The electrode materials were symbolized as NCIMs (nanocrystallite-insertion-materials). Indeed, by minimizing the crystallite size, we favor the formation of dangling and weak bonds at the surface and, thereby, the rate of reversible lithium insertion. Since the previously studied NCIMs were based on transition metal oxides, we were more concerned in earlier publications in the cationic "d" orbitals that were involved in the electrochemical processes[15-17]. In the case of SnO_2 based electrodes, it is the cationic "5s" orbitals that would be of concern; as for WO_3, the "5d" orbitals are involved. Therefore, it is worthwhile to have an insight into the respective influences of "s" and "d" orbitals on the electrochemical response using SnO_2 and WO_3 as examples. The SnO_2 powders were prepared by both methods 1 and 2 for comparison; the WO_3 powders were obtained by method 2.

EXPERIMENTAL

Sample preparation

a) Method 1

A colloidal stannic hydroxide was precipitated by the dropwise addition of ammoniacal solution (35%, Aldrich) to an aqueous solution chloride (99.99%, Aldrich) maintained at ~ 2°C in an ice-water bath. Residual impurities of hydrogen chloride and ammonium chloride were removed by repeatedly washing with distilled water. The washing and filtering process were repeated until the pH of the solution decreased to 7.5 (from an initial value of 12.5). The as-obtained α-stannic acid gel was heated in dry oxygen for 2h at different temperatures (150, 350 and 550°C) in order to get powdery samples with different morphologies. The heating and cooling temperature rate (1°C/min) was controlled using a Eurotherm programmer. The samples are identified hereafter as 1-(150); 1-(350); 1 ≠ (550) "1" designates the method of preparation and the number within brackets represents the heat treatment temperature.

b) Method 2.

Four grams of polyethylene oxide (PEO: Aldrich, M. W. 500,000) was first added to 230 ml of acetonitrile. Immediately afterwards, $SnCl_4.5H_2O$ or WCl_6 (Aldrich, 99.99%) were added to the solution in the proportions $[-CH_2-CH_2-O]/M = 8$, (M = Sn or W). The solution was stirred at room temperature for about 6 hrs, i.e., until a satisfactory homogeneity was achieved. Then, the 'sol' was cast in a teflon mould. Evaporation of the solvent at about 40°C under a stream of dry air gave an organo-metallic polymer film of typical thickness 100μm. Finally, fine-grained SnO_2 and WO_3 powders were obtained by eliminating the C, H elements of the polymer film with slow heating in dry oxygen. In order to get NCIMs (with different morphologies, the polymer films were heated up to 350°C, 450°C, or 550°C and soaked for 2hrs at those temperatures. The heating and cooling temperature rate value was 1°C/min.

The powdery SnO_2 and WO_3 samples are identified as 2-(350), 2-(450), 2-(550) and 2-(350)W, 2-(450)-W 2-(550)-W; as above, "2" designates the method of preparation and the number within brackets the temperature of heat treatment. the symbol "W" identifies the tungsten oxide samples.

The preparation procedure involved in methods 1 and 2 are schematically illustrated in Fig. 1. Let us note that the time required for the synthesis of the powders using the method 2 is much shorter (about 2/3 shorter) than that required for method 1: indeed, the filtering and milling processes intervene only in method 1.

Sample analysis:

Thermogravimetric analyses, using a Leco TGA-501 display, were performed in dry air between 22°C and 600°C with a Setaram thermobalance. X-ray diffraction measurements were obtained with a Phillips PW 1050 spectrometer and CuK_α

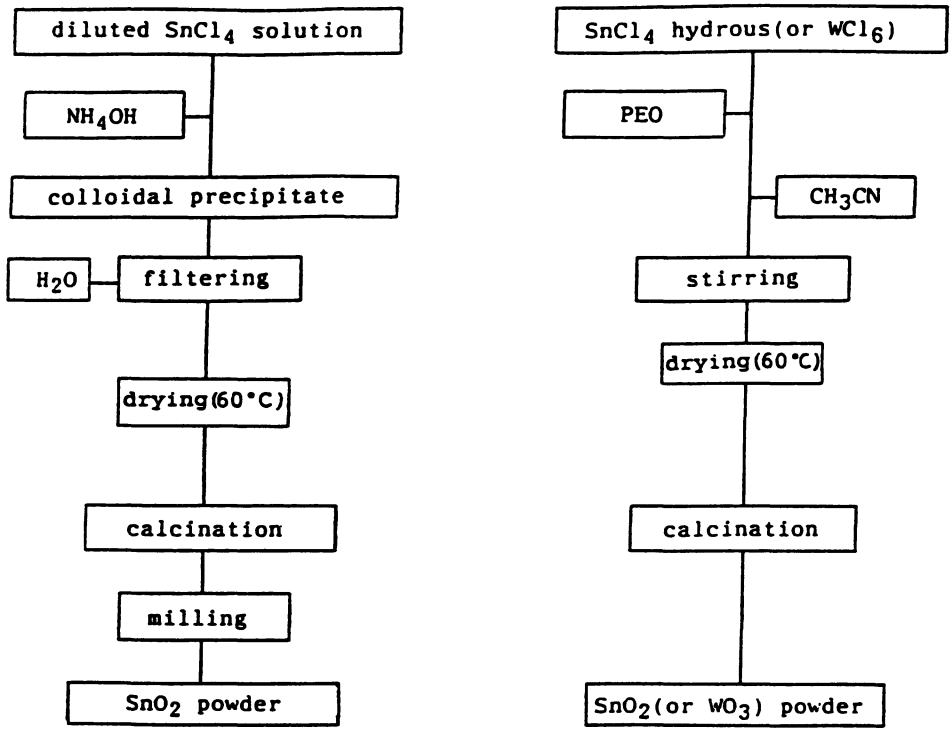

FIGURE 1 Schematic diagrams of the steps involved in obtaining fine-grained SnO_2 and WO_3 powders.

radiation. The average crystallite size, D, was calculated from the well known Scherrer's formula

$$D = 0.9\lambda/\beta_{1/2} \cdot \cos\theta \tag{1}$$

$\beta_{1/2}$ is the corrected width of the main diffraction peak at half height, λ is the X-ray wavelength, and θ the diffraction angle. The specific surface area of the samples was measured using the single point Brunauer Emnett and Teller (BET) method with a Micromeretics Accu Sorb 2100 E. The samples were outgassed at 180°C for 5 hrs. The adsorbate gas was nitrogen. The IR spectra in the adsorbance mode were recorded on a Perkin-Elmer 983G spectrometer between 4000 and 200 cm^{-1} with an average resolution of 5 cm^{-1}. The experiments were performed on SnO_2 and WO_3 powders dispersed in Nujol and sandwiched between two cesium iodide disks. Conductivity experiments using the Van der Pauw four probe technique were carried on using samples that were pressed at 5 tons/ cm^2 in a steel die of diameter 13 mm. The analysis of the carbon content and the composition of the gases released during the sample pyrolysis were achieved using the TGA

apparatus equipped either with an elemental analyser (LECO, CHN-1000) or with a gas chromatograph (Varian 3700).

Electrochemical measurements:

Electrochemical (de)insertion of lithium was realized in bottle-type cells having two electrodes. The cathode consisted of 35 mg of SnO_2 or WO_3 powder and 6 mg of carbon black (i.e. $\sim$ 15w%). The cathode was prepared by intimately mixing the powders (previously outgassed at 180°C for 5 hrs) and pressing in the form of a disk in a 1.3 cm diameter stainless steel die. Lithium metal was used as both reference and anode. The electrolyte was a 1M $LiCF_3SO_3$-propylene carbonate solution impregnated into a glass filter paper. The propylene carbonate (Aldrich 99 + %) was further dried by fractional distillation under 4Å molecular sieves. The lithium triflate (Aldrich 97%) was kept under vacuum at 150°C during 72 hrs. The experiments were then carried out inside a glove box maintained under argon atmosphere and containing less than 1 ppm H_2O and O_2.

RESULTS AND DISCUSSION

Sample composition

a) Samples 1-(150), 1-(350), 1-(550)

The presence of adsorbed water hydroxyl groups in samples 1-(150) and 1-(350) is also revealed in the IR spectra (fig. 2). Adsorbed water is best characterized by its deformation mode δOH_2 occurring near 1620 cm^{-1} 18,19. This adsorption band is only observed in sample 1-(150). The broad features between 3500 and 3100 cm^{-1} observed for samples 1-(150) and 1-(350) can involve stretching modes of water, hydroxyl groups. Traces of ammonium ions arising from the synthesis might also occur and contribute to the previous broad adsorption (ν_1 and ν_2 modes of NH_4^+)[20,21]. However, nothing is detected around 1420 cm^{-1} (ν_4 mode of NH^{4+}).

On the other hand, a weak and broad feature is observed at about 1200 cm^{-1} in both 1-(150) and 1-(350) samples. It can be attributed to a hydroxyl bending mode. It can be attributed to a hydroxyl bending mode. Therefore, for sample 1-(350), which presents no water adsorption at 1620 cm^{-1}, it can be concluded that the protons are essentially involved in hydroxyl groups and the broad high frequency adsorption reflects mainly the stretching vibrations of these hydroxyl groups.

Finally, sample 1-(550) exhibits neither water nor hydroxyl group vibrations.

It is known that the presence of hydroxyl groups and adsorbed water in fine-grained SnO_2 powders favors protonic conductivity[22,23]. The latter can be evidenced from d.c. conductivity measurements, as shown below. First of all, the d.c. electric induced by an applied potential of 1 V across a disk of SnO_2 (1 mm thickness, 13 mm diameter) is shown in fig. 3 gold electrodes that are blocking to ionic motion insure the electrical contacts. The term "blocking to ionic motion" means the absence of any ionic transfer via the interfaces between the electrodes and the electrolyte.

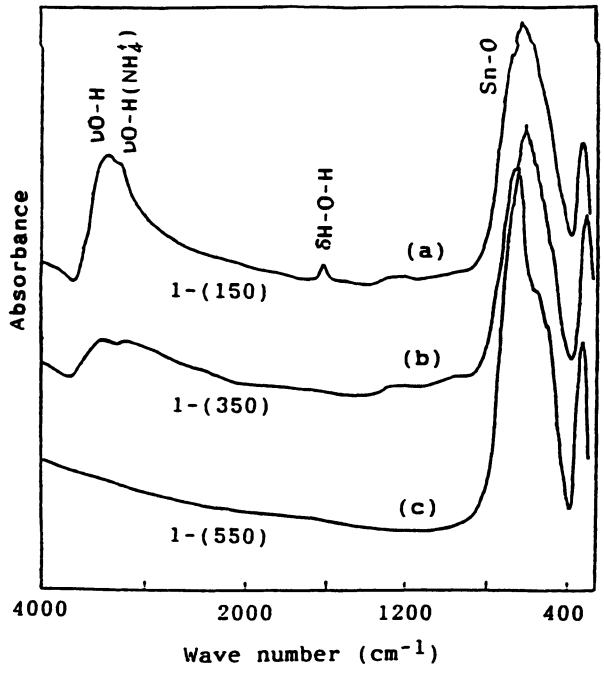

FIGURE 2 IR absorption spectra of (a)1-(150), (b)1-(350) and (c)1 – (550) samples.

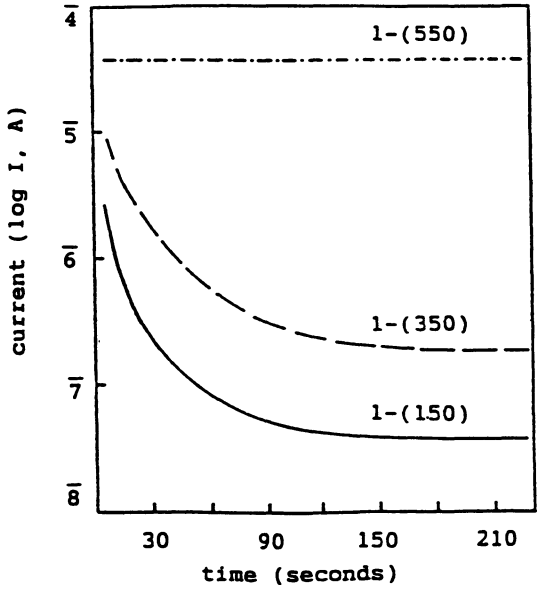

FIGURE 3 Electrical current across a pressed pellet (d_{exp}, $/d_{theor.}$ = 55%) of SnO_2 prepared employing method 1 and for an applied potential of 1 V.

With the blocking electrodes, the protonic conductivity causes the "polarization effect" illustrated in fig. 3 for samples 1-(150) and 1-(350): it can be noted that the current measured immediately after the potential has been applied is time dependent, accounting for an ionic (i.e., protonic) conductivity. The large concentration of the mobile enables, indeed, the progressive accumulation of a large number of charges within a thin thickness at the interfaces, causing the observed decrease of the current between 0 and 150 s (fig. 3). We are dealing, in fact, with the well known phenomena of the double electrical layer that which is produced at the blocked interface between an electronic conducting electrode and an ionic conductor. When $t > 150$s, the interfaces are built and the observed residual steady current (fig. 3) account for a residual electronic conductivity. The occurrence of protonic conductivity in samples heated only up to 350°C has also been observed by others[25-26]. The constant current, observed uniquely for sample 1-(550) within the whole time range (fig. 3), accounts for the expected absence of ionic conductiv-

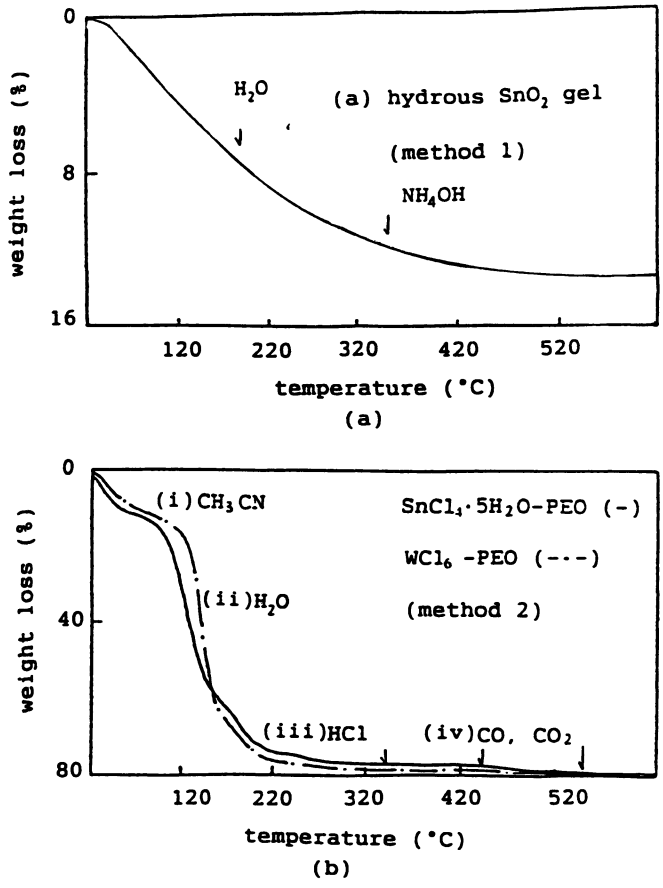

FIGURE 4 TGA profiles of hydrated SnO_2 gel (a), $SnCl_4 \cdot 5H_2O$-PEO and WCl_6-PEO (b), recorded in dry air with a heating rate of 1°C per minute.

TABLE 1

Sample characteristics according to the preparation conditions.

Preparation procedure	Method 1			Method 2					
	SnO_2			SnO_2			WO_3		
Samples	1-150	1-350	1-550	2-350	2-450	2-550	2-350-W	2-450-W	2-550-W
'*n*' value in $SnO_2 \cdot nH_2O$ $WO_3 \cdot nH2O$	1.5	0.5	0.0	0.0	0.0	0.0	0.0	0.0	0.0
Content carbon(wt%)	0.0	0.0	0.0	~ 15	~ 5	0.0	~ 10	< 5	0.0
Colour	white	pale yellow	pale yellow	black	brown	grey white	black	brown	pale green

ity (and hence of hydroxyl groups or adsorbed water). Moreover, the higher current observed for this sample results from an increased electronic conductivity due to an increase in concentration of oxygen vacancies. The latter introduce, indeed, ionized electronic donor centers that are responsible for an enhanced electronic conductivity[26].

Even though a small amount of ammonia not detectable by IR spectroscopy might occur, the compositions of samples 1-(550), 1-(350) and 1-(550) have been from the general formula SnO_2-nH_2O[27]. The *n* values have been deduced from TGA measurements (fig. 4a); they are reported in table I,

b) Samples 2-(350), 2-(450), 2-(550); 2-(350)-W, 2-(450)-W and 2-(550)-W

As reported above, the powdry SnO_2 and WO_3 samples result from the calcination of polymer-metal halide complexes at the required temperatures (350°C, 450°C, 550°C). The corresponding overall weight loss, as evidenced from TGA studies, is about 80%: it takes place in four stages as depicted in fig. 4b. The initial weight loss of ~ 12%, stage (i), is completed below ~ 100°C. It corresponds to the evaporation of the residual CH_3CN solvent. The stages (ii) and (iii) are completed between ~ 130 and 200°C and ~ 300°C respectively, they account for the emission of H_2O and HCl (~ 65%weight loss). The last step (iv) is completed at ~ 500°C, it corresponds to the departure of CO, CO_2 traces (~ 3% weight loss). Traces of carbon remaining in samples 2-(350), 2-(450), 2-(350)-W and 2-(450)-W give them a dark coloration (table 1), therefore IR spectroscopy measurements cannot be carried out. However TGA measurements reveal no measurable traces of water and hydroxyl groups in all samples. Consequently, the SnO_2 and WO_3 powders are likely to behave as the (quasi) water free and hydroxyl group free NCIMs whose electrochemical Li^+ (de)insertion efficiency has already been demonstrated by some of us[15–17]. To prove the occurrence of the similarity in the behavior of the SnO_2 and WO_3 powders to those of the NCIMs, we have to examine first the crystalline structure and texture prior to any electrochemical investigation.

Crystalline structure and texture:

X-ray diffraction measurements were carried out on all samples listed in table 1 in order to know the evolution of the crystalline size as a function of calcination

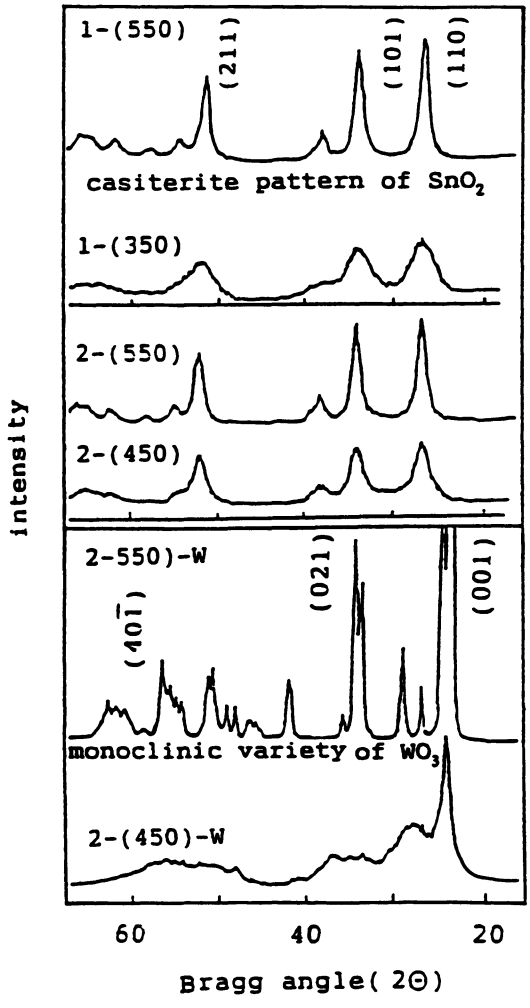

FIGURE 5 X-ray diffractograms of some SnO_2 and WO_3 powders.

temperature. For the sake of clarity, the diffractograms, which are the most representative of this evolution, are shown in fig. 5. The X-ray diffraction lines are very broad for 1-(350), 2-(450) and 2-(450)-W. However, their presence indicates that the samples are nanocrocystalline in nature rather than glasses. The main size, D, of the microcrystallites, listed in table 2, were estimated by considering the diffraction broadening of the peaks corresponding to the (110) plane for tin oxide and to the (001) plane for tungsten oxide.

We compare in table 2 the specific surface areas of the SnO_2 powders 1-(550) and 2-(550) having rather similar crystallite size and being free from contamination by water and/or hydroxyl groups and carbon (originating from PEO). Most interestingly, a much higher value is obtained for the sample 2-(550). Consequently, prior to its complete departure, the organic part restrains the crystallite

TABLE 2

Evolution of the crystallite size and specific surface area with calcination temperature using both methods 1 and 2.

Samples	1-150	1-350	1-550	2-350	2-450	2-550	2-350-W	2-450-W	2-550-W
Crystallite (a) size (±6Å)	< 20	30	75	< 20	45	70	< 30	60	308
(110) (b)	25	55	150	–	–	–	–	–	–
Surface (a) area (m^2/g)	122	148	39	16	104	75	16	38	25

(a) this study: let us quote that the surface areas reported here are related to the particle size and pore volume (the accepted definition being that many crystallites make a particle).
(b) from references 28-30

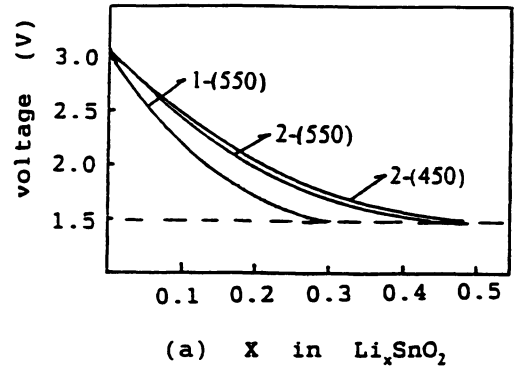

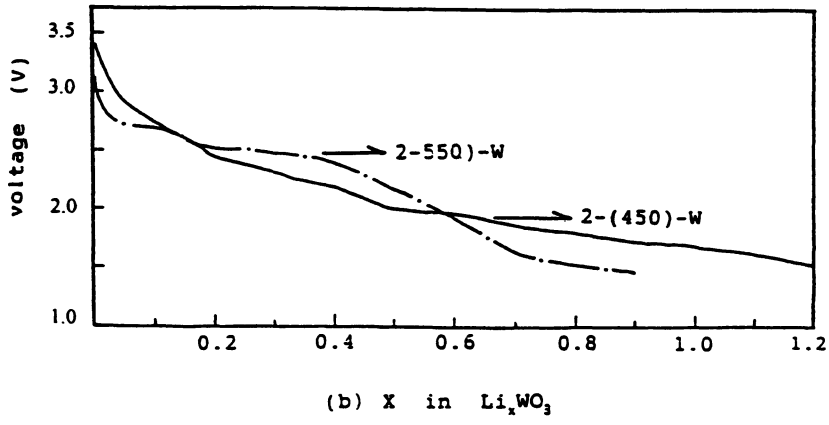

FIGURE 6 Reversible 10th discharge curves of (a) $Li/Li^+/Li_xSnO_2$ and (b) $Li/Li^+/Li_xWO_3$ cells between voltage limits of 1.5-3.1V (a), and of 1.8-3.1V (b), vs Li. The current density was $50\mu A/cm^2$ for an electrode weight of 35 mg.

and particle growth. The crystallite and particle growths are, indeed promoted only when the organic part is almost eliminated. As expected, the specific area increases as the crystallite size is reduced, from 2-(550) to 2-(450) on the one hand, and from 2-(550)-W to 2-(450)-W, on the other hand (table 2). Finally, the low surface area values reported in table 2 for samples 2-(350) and 2-(350)-W are due to the incomplete elimination of the polymer-residuals at 350°C; the carbon content (measured using atomic adsorption spectroscopy) is indeed as high as 15% (table 1). It may be possible that the SnO_2 and WO_3 crystallites are bound together through O-C bonds; consequently very small surface areas are observed for 2-(350) and 2-(350)-W.

Electrochemistry: influence of grain and particle sizes on the reversible electrochemical insertions of lithium in SnO_2 and WO_3 NCIM electrodes:

As pointed out above in the experimental part, the obtained samples were intercalated with lithium in the following electrochemical cells: $Li/LiCF_3SO_3$ in propylene carbonate$/SnO_2$ and $Li/LiCF_3SO_3$ in propylene carbonate $/WO_3$. The measurements were carried out at room temperature. The lithium insertion process was conducted, using the well known cyclic manner, by (dis)charging the cells with a constant current of 50 $\mu A/cm^2$.

Fig. 6 illustrates the reversible 10^{th} discharge curves of the cells for the samples free from contamination by water, hydroxyl groups, and residues of PEO (table 1). In agreement with our model[15–17], the highest rate of lithium insertion occurs for the NCIMs 2-(450) and 2-(450)-W, which possess the highest specific surface area. Our results concerning WO_3 are also in argreement with Zhang[31] who showed that powdery Li_xWO_3 electrodes having surface areas of $4.3m^2/g$ and $12.2m^2/g$ reversibly insert $x = 0.28$ and $x = 0.48$ lithium, respectively, between 1.8 and 3.2 V vs Li. In our work, the rate of lithium reversibly inserted is higher ($x = 1.2$ for 2-(450)-W) because of the higher specific surface area. Within the same voltage range (fig. 6), the amount of Li inserted is larger in the case of WO_3 compared to SnO_2: it is indeed related to the electron affinity of the W^{6+}/W^{5+} couple, which is larger (in absolute value) than that of the Sn^{4+}/Sn^{2+} couple. Fig. 7 illustrates the good cycling reversibility observed for 2-(450) and 2-(450)-W electrodes.

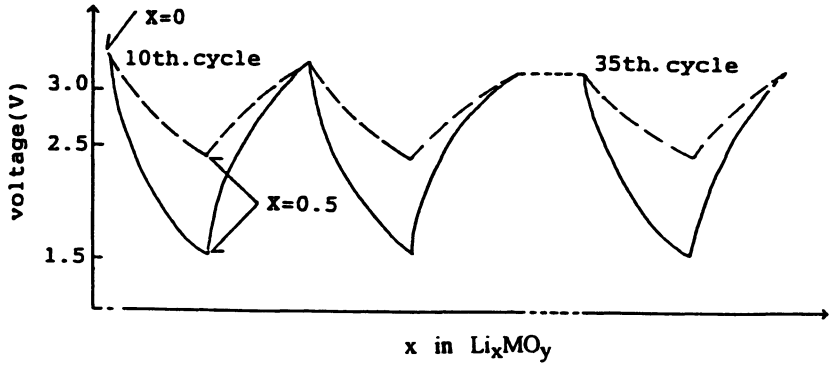

FIGURE 7 Series of charge-discharge curves for $Li/Li^+/Li_xSnO_2$(—) and $Li/Li^+/Li_xWO_3$ (-----) cells using 2-(450) and 2-(450)-W electrodes (I-50μA; electrode weight = 35 mg).

CONCLUSIONS

In this paper we have distinguished two methods for preparing fine-grained tin oxide powders. The method 2, to our knowledge, seems to be original and leads to SnO_2 powders free from water and/or hydroxyl groups and with small crystallite and particle sizes. Method 2 also has been used to prepare powdery WO_3 samples having the finest crystallites. Related to the fine-grained texture of the samples, we have shown that they are able to sustain long-term electrochemical cyclability. In fact, they behave like other NCIMs that we have recently investigated[17]. Indeed, by minimizing the size of the crystallites, the formation of defect bonds is favored, particularly at the crystallite surface, acting as reversible grafting sites for Li^+. Moreover, the cation-anion bonding would be weakened not only in the grain boundary region, but also within a grain close to its surface. Therefore, the electrochemical insertion of Li^+ would also occur through an easy bonding rearrangement.

Let us point out that for WO_3 these "non-conventional" insertion mechanisms should occur in addition to the well known intercalation mechanisms of Li within the crystallites and allowed by their tunnel type structure. However, in order to check the validity of the discussions and conclusions made here, further investigations of *in situ* IR and Raman spectroscopy and of the evolution of the electrode-equilibrium potentials as a function of the Li insertion rate are necessary.

REFERENCES

1. E.E. Kohnke, J. Phys. Chem. Solds 23 (1962) 1557.
2. W. Spence, J. of Applied Physics, 38 (1967) 398.
3. K.L. Chopra, S. Major, D.K. Pandya, Thin Solid Films, 102 (1983) 1.
4. C. Kemball, H.F. Leach, I.R. Shannon, J. Catalysis, 29 (1973) 99.
5. J. L. Aucouturier, P. Hagenmuller, J. Portier, J. Salardenne et al., Proc. 2nd Intl. Conf. on Chemical Sensors, Bordeaux, France (1986).
6. M. Mizumoto, H. Yamashita, S. Matsuda, Ind. Eng. Chem. Prod. Res. Dev. 24 (1985) 12.
7. M.J. Fuller, M.E. Warwick, J. of Catalysis 29 (1973) 102.
8. M. Itoh, H. Hattori, K. Tanabe, ibid 43 (1976) 78
9. K.F. Poulter, J.A. Pryde, Brit. J. Appl. Phys. Ser. 1 (1968) 169
10. F. Harb, B. Gerand, G. Nowogrocki, M. Figlarz, Solid State Ionics 32/33 (1989) 16.
11. K.H. Cheng, A.J. Jacobson, M.S. Wittingham, ibid 5 (1981) 26.
12. K.H. Cheng, M.S. Wittingham, ibid 1 (1980) 120.
13. Q. Zhong, J.R. Dahn, K. Colboro, J. Electrochem. Soc. 139 (1992) 195.
14. P.V. Wright, Brit. Polymer J., 7 (1975) 319.
15. B. Morrel, Doctoral Thesis, University of Bordeaux, France, (1991).
16. S.D. Han, G. Campet, J. Portier, C. Delmas and J. C. Lassegues in Proc. of GFECI meeting in Clermont-Ferrand (1993) 15.
17. G. Campet, S.J. Wen, S.D. Han, M.C.R. Shastry, J. Portier, Mat. Sci. Eng. B. 18 (1993) 201 and references therein.
18. E.W. Thortnon, P.G. Harrison, Trans. Faraday Soc. 171 (1975) 461.
19. Braune and Knoke, Z. Phisik Chem., 135 (1928) 49.
20. Landolt-Bronstain, Physikalisch-Chemeche Tabellen, 2 Teil (1975).
21. W. Vedder, D.F. Hornig, J. Chem. Phys. 35 (1961) 1560.
22. J.A. Chapman and E. Lilly J. Phys. C 934 (1973) 455.
23. G.N. Greaves, J. Non-Cryst. Solids 11 (1973) 472.

24. C. Geoffroy, G. Campet, F. Menil, Active and Passive Electron. Comp. 14 (1991) 111.
25. L.L. Hench, "Physics of Electronic Ceramics", M. Dekker, New York (1971) 524–537.
26. P. Colomban, "Proton conductors," Cambridge univ., U.K. (1992) 418–431.
27. W.A. England, M.G. Cross, J. B. Goodenough, Solid State Ionics, 1 (1980) 231.
28. J.J. Goodman and S.J. Gregg, J. Chem. Soc. (1960) 1162.
29. M.J. Fuller, M.E. Warwich, A. Walton, J. Appl. Chem. Biotecnol. 28 (1978) 369.
30. S. Kittika, K. Morishige, T. Fujimoto, J. Coll. Inter. Sci. 72 (1972) 191.
31. Q. Zhang, J.R. Dahn, K. Colbow, J. Electrochem. Soc., 139 (1992) 2046.

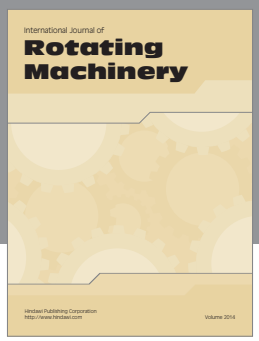

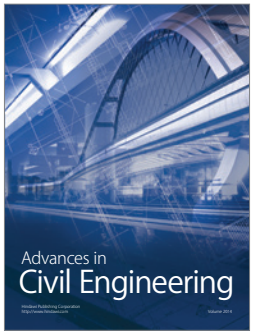

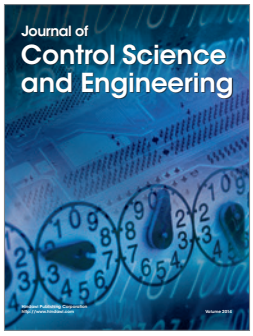

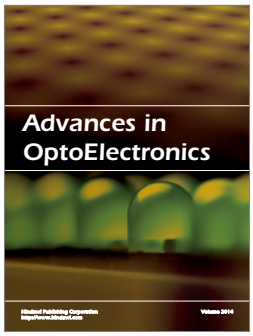

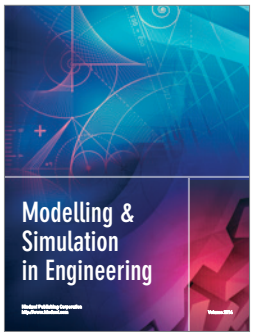

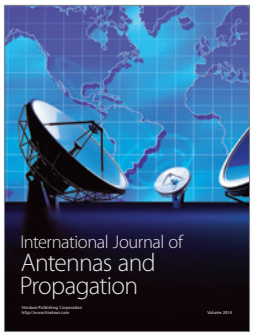

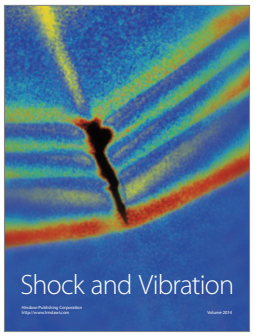

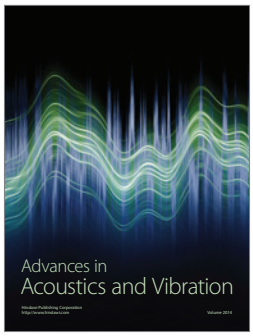

Hindawi

Submit your manuscripts at
http://www.hindawi.com